Understanding the effects of pre-processing on extracted signal features from gait accelerometry signals

Alexandre Millecamps[1], Jennifer S. Brach[2], Kristin A. Lowry[3], Subashan Perera[4], Mark S. Redfern[5], Ervin Sejdić [1,*]

Abstract

Gait accelerometry is an important approach for gait assessment. Previous contributions have adopted various pre-processing approaches for gait accelerometry signals, but none have thoroughly investigated the effects of such pre-processing operations on the obtained results. Therefore, this paper investigated the influence of pre-processing operations on signal features extracted from gait accelerometry signals. These signals were collected from 35 participants aged over 65 years-old: 14 of them were healthy controls (HC), 10 had Parkinson's disease (PD) and 11 had peripheral neuropathy (PN). The participants walked on a treadmill at preferred speed. Signal features in time, frequency and time-frequency domains were computed for both raw and pre-processed signals. The pre-processing stage consisted of applying tilt correction and denoising operations to acquired signals. We first examined the effects of these operations separately, followed by the investigation of their joint effects. Several important observations were made based on the obtained results. First, the denoising operation alone had almost no effects in comparison to the trends observed in the raw data. Second, the tilt correction affected the reported results to a certain degree, which could lead to a better discrimination between groups. Third, the combination of the two pre-processing operations yielded similar trends as the tilt correction alone. These results indicated that while gait accelerometry is a valuable approach for the gait assessment, one has to carefully adopt any pre-processing steps as they alter the observed findings.

Keywords: Gait accelerometry, signal features, pre-processing effects, Parkinson's disease, peripheral neuropathy, healthy controls.

*Corresponding author

[1]Department of Electrical and Computer Engineering, Swanson School of Engineering, University of Pittsburgh, 3700 O'Hara Street, Pittsburgh, PA, USA, 15261. Phone: 412-624-0508. E-mail: esejdic@ieee.org

[2]Department of Physical Therapy, University of Pittsburgh, Pittsburgh, PA, 15260, USA.

[3]Deparment of Physical Therapy, Des Moines University, Des Moines, IA 50312, USA.

[4]Department of Medicine, Division of Geriatrics, University of Pittsburgh, Pittsburgh, PA, 15261, USA.

[5]Department of Biomedical Engineering, Swanson School of Engineering, University of Pittsburgh, Pittsburgh, PA, 15261, USA.

1. Introduction

Maintaining balance is a challenging activity for the human body, which is an unstable system if not continuously controlled [1], and an increased impairment of the balance control system corresponds to an increase of gait impairments [2, 3]. This highlights the need for clinicians to assess patients' gait. Clinicians attempt to accurately describe the health state of a patient via gait analysis in order to diagnose a gait disorder or to decide on a treatment that may improve patients' gait [4, 5]. When dealing with elderly patients, the assessment of balance while standing and walking has proved to be a predictor of falls [6] and is related to self-rated health status [7], cognitive impairment caused by dementia [8, 9], mortality and morbidity [10, 11].

Over the years, several approaches have been employed to assess gait. In particular, previous publications have utilized various measurements systems for gait assessment such as camera systems (e.g., [12, 13]), body-mounted accelerometers (e.g., [14, 15, 16, 17, 18, 19, 20, 21, 22]), force platforms (e.g., [1], [13, 23]) and gyroscopes (e.g., [24, 25, 26]). Force platforms and cameras have the advantage of providing a fixed frame of reference whereas body-mounted systems enable subjects to cover longer distances [14].

Gait accelerometry has become a widely adopted approach [27] due to its reliability, high precision and affordability [28]. It also enables computing a wide range of metrics to evaluate gait [29, 30, 27, 31]. Pre-processing of gait-accelerometry signals may be necessary to remove noise or minimize the effect of gravity [14]. In previous publications it has been argued that a correction of the acceleration measurement is necessary due to the spine lordosis in the L3 region, the imprecise positioning of the accelerometer, and the effect of the gravity component over the measured accelerations [14]. Previous contributions also noticed that gait acceloremtry signals can be noisy, and some denoising pre-processing may be needed in order to be able to extract gait features (e.g., [32, 33]). However, pre-processing can have unintended consequences such as determining potential group differences when they do not exist. It is therefore logical to question the impact of pre-processing on the extracted gait features.

A multitude of processes can be applied to the acquired signals. In this study, we applied two pre-processing operations used in gait analysis (e.g., [14, 31, 32, 33, 34, 35]): tilt correction and wavelet denoising. As these are commonly applied pre-processing operations on gait accelerometry signals, the purpose of this paper was to understand their influence on signal features calculated in time, frequency and time-frequency domains using signals from different populations in order to understand whether pre-processing operations have detrimental effects on our ability to discriminate amongst pathological groups. We first extracted features from the raw signals. Then, we examined the effects of tilt correction on the extracted features, followed by the effects of denoising on the extracted features. Lastly, we examined the effects of

joint pre-processing, i.e., we applied both operations (correction and denoising) to the raw data. However, to understand whether the order of operations play a significant role, we examined these effects using a two-step approach. In the first step, we corrected data followed by the denoising operation. In the second step, we denoised the data initially, followed by the correction operation.

Additionally, we explored whether the pre-processing operations affected the calculated acceleration features differently in individuals with and without expected gait abnormalities by examining individuals with Parkinson's disease (PD), peripheral neuropathy (PN) and healthy older adults. The possible presence of tremor, rigidity, and spinal inflexibility [36] in PD may impact both the position of the accelerometer and signal quality. Similarly, persons with PN typically walk with a wider base of support [37], which also may impact accelerometer recordings. Thus, pre-processing operations may have a greater impact on the values of the extracted acceleration features for these clinical groups. As use of acceleration-based outcomes measures is gaining grounds in rehabilitation randomized controlled trials, it is imperative that the signal processing methodology becomes standardized, otherwise it will become difficult to comparatively analyze the results of different trials.

The major contribution of this manuscript is our finding that pre-processing has an impact on extracted gait accelerometry features especially after the application of tilt correction. It was important to understand whether pre-processing schemes have detrimental effects on our ability to gain discriminate across pathological groups, as no previous contribution has ever examined the effects of pre-processing operations on features extracted from gait accelerometry signals. However, we need to point out that the manuscript focuses on two commonly used pre-processing schemes for gait accelerometry signals, and it is beyond the scope of the current manuscript to comprehensively analyze all pre-processing approaches typically found in other areas.

2. Methods

2.1. Data acquisition

A total of 35 patients aged 65-year-old and older were enrolled in the experiment: 14 were healthy controls (HC), 10 had Parkinson's disease (PD) and 11 had peripheral neuropathy (PN). All of them could walk without human or mechanical assistance for at least 3 minutes. Details of participant have been reported in a previous study [31]. All subjects were assessed using a structured history and physical exam to ensure they met the general inclusion/exclusion criteria for the study. Potential subjects were excluded if they had any undiagnosed neurological (e.g. abnormal neurological examination such as spasticity, or severe paresis), musculoskeletal or cardiopulmonary conditions or inadequate hearing or vision that would interfere

with walking. Additionally, eligibility for HCs required no diagnosed neurological, vestibular or sensory disorders plus biothesiometer reading at the malleolus < 20 v bilaterally. PDs had established neurologist diagnosis of Parkinson's disease for at least one year according to Hoehn and Yahr scale rating of 2 or 3 and a bioesthesiometer measure reading at the malleolus < 20 v bilaterally. Subjects were on a stable dosing schedule of Parkinson's medications for the prior three months. Subjects with PN had biothesiometer readings of ≥ 40 v bilateraly, indicating lose of vibratory sense. Subjects meeting the inclusion criteria completed the baseline assessments that included an overground walk used to determine self-selected treadmill speed.

Subjects meeting the inclusion/exclusion criteria walked on a computer-controlled treadmill (1.2 m wide by 2 m long). Safety was ensured by a harness system. An accelerometer was attached firmly to each patient over the L3 segment of the lumbar spine using a belt and a 4-inch wide elastic bandage wrapped over the accelerometer and the trunk. Linear accelerations were measured along the medial-lateral (ML), vertical (V) and anterior-posterior (AP) directions and sampled at 100 Hz. Participants completed walking trials at their preferred speed (i.e., their comfortable walking speed). To establish preferred speed, the treadmill speed was incrementally increased (e.g., 0.05 0.10 m/s) until a participant reported a comfortable walking speed. Comfortable walking speeds were re-established for each participant by increasing and decreasing treadmill speed [38]. At the beginning of each walking trial there was a ramp up period during which the subject's walking speed was slowly increased until their previously established preferred pace was reached. After being accustomed to the instrumentation as well as walking on the treadmill, the subjects performed a 3-minute walk at a desired (usual) pace. The average treadmill speed was 1.06 ± 0.014 m/s ranging from 0.74 m/s to 1.30 m/s. No treadmill tilt was used in this experiment.

2.2. Data pre-processing

Dynamic tilt correction. In previous publications concerning gait analysis while walking [14, 39], it has been argued that a correction of the acceleration measurement is necessary due to the spine lordosis in the L3 region, the imprecise positioning of the accelerometer, and the effect of the gravity component over the measured accelerations. We performed tilt correction using the method developed by Moe-Nilssen [14]. Coordinates of the accelerometer were rotated to earth-vertical (Figure 1).

The accelerometer is situated near the L3 lumbar vertebra which minimizes the transverse plane offset rotation of the device. Therefore we assume that the AP acceleration is situated in the sagittal plane. θ_{AP} and θ_{ML} are the angles between the transverse plane and the measured accelerations. $\mathbf{a}_{H-AP}$ and $\mathbf{a}_{H-ML}$ are projections of the measured accelerations in the new coordinate system. $\mathbf{a}_{V'}$ is the temporary corrected vertical acceleration i.e the acceleration after correcting the measured one in the AP plane and $\mathbf{a}_V$ is the

vertical acceleration in the new coordinate system. Angles are positive above the horizontal axis and positive axes are horizontal to the right and vertical up.

The following equations operate the coordinate transform:

In the sagittal plane

$$\mathbf{a}_{H-AP} = \mathbf{a}_{AP}\cos(\theta_{AP}) - \mathbf{a}_{v}\sin(\theta_{AP}) \tag{1}$$

$$\mathbf{a}_{V'} = \mathbf{a}_{AP}\sin(\theta_{AP}) + \mathbf{a}_{v}\cos(\theta_{AP}) \tag{2}$$

In the coronal plane

$$\mathbf{a}_{H-ML} = \mathbf{a}_{ML}\cos(\theta_{ML}) - \mathbf{a}_{V'}\sin(\theta_{ML}) \tag{3}$$

$$\mathbf{a}_{V} = \mathbf{a}_{ML}\sin(\theta_{ML}) + \mathbf{a}_{V'}\cos(\theta_{ML}) - \mathbf{g} \tag{4}$$

where $\mathbf{g}$ is the gravity vector. Since the acceleration unit is g, we have $\mathbf{g} = 1$.

Moe-Nilssen [14] showed that the quantities $\sin(\theta_{AP})$ and $\sin(\theta_{ML})$ can be approximated by the mean of the accelerations in the AP and ML directions respectively for a large number of samples. The i^{th} sample in the j^{th} anatomical direction $\mathbf{a}_{i,j}$ (with $j = \{\text{AP, ML}\}$) can indeed be decomposed in two terms: one is the measured change of velocity $\mathbf{a}_{\text{c}(i,j)}$, the other is the static gravity component $\mathbf{a}_{\text{g}(i,j)}$:

$$\mathbf{a}_{\text{(i,j)}} = \mathbf{a}_{\text{c}(i,j)} + \mathbf{a}_{\text{g}(i,j)} \tag{5}$$

The expected value of the measured accelerations can be expressed as follows:

$$E[\mathbf{a}_{(i,j)}] = \lim_{n\to\infty} \frac{1}{n}\sum_{i=1}^{n} \mathbf{a}_{(i,j)} \approx \overline{\mathbf{a}}_{j} \tag{6}$$

Replacing the acceleration by the expression of a velocity change leads to the following expression:

$$\begin{aligned} E[\mathbf{a}_{\text{c}(i,j)}] &= \lim_{n\to\infty} \frac{1}{n}\sum_{i=1}^{n} \mathbf{a}_{\text{c}(i,j)} \\ &= \lim_{n\to\infty} \frac{1}{n+1}\sum_{i=1}^{n+1} \frac{v_{(i,j)} - v_{(i-1,j)}}{\Delta t} \\ &= \lim_{n\to\infty} \frac{v_{(n+1,j)} - v_{(1,j)}}{(n+1)\Delta t} = 0 \end{aligned} \tag{7}$$

where Δt denotes the sampling time. Assuming θ_j is constant we have:

$$E[\mathbf{a}_{\text{g}(i,j)}] = \lim_{n\to\infty} \frac{1}{n}\sum_{i=1}^{n} \mathbf{a}_{\text{g}(i,j)} = \mathbf{a}_{\text{g}(i,j)} \tag{8}$$

since the gravity vector is constant. Recalling equation 5, we have

$$E[\mathbf{a}_{(i,j)}] = E[\mathbf{a}_{\text{c}(i,j)}] + E[\mathbf{a}_{\text{g}(i,j)}] = E[\mathbf{a}_{\text{g}(i,j)}] \tag{9}$$

Hence

$$\overline{\mathbf{a}}_j = \mathbf{a}_{g(i,j)} \tag{10}$$

The gravity vector can be decomposed according to the measured accelerations:

$$\mathbf{g} = -\sin(\theta_{AP})\mathbf{a}_{AP} + \cos(\theta_{AP})\mathbf{a}_v \tag{11}$$

Finally, the approximation of the angles for a large number of samples is given by:

$$\overline{\mathbf{a}}_j = \sin(\theta_j) \tag{12}$$

Once these values are known, the estimated accelerations can be calculated.

Wavelet denoising. Gait accelerometry signals can be corrupted by noise generated by the measurement device. Therefore, a 10-level discrete wavelet transform using Meyer's discrete wavelet and soft thresholding [40] was applied to the data. The wavelet analysis is a signal processing tool used to complement the Fourier analysis for understanding the nonstationary nature of many signals, especially biomedical signals (e.g., [41, 42, 43, 44, 45]).

Indeed the Fourier transform decomposes a signal in terms of complex exponential functions $e^{i\omega t}$ using the following formula:

$$\hat{f}(\omega) = \int_{-\infty}^{+\infty} f(t)e^{-i\omega t}dt \tag{13}$$

where f is a signal and $\hat{f}$ its Fourier transform.

In wavelet theory, the complex exponential function is replaced by a function $\psi(t)$ called the *mother wavelet* having defined characteristics [46]:

$$\int_{-\infty}^{+\infty} |\psi(t)|dt = 0 \tag{14}$$

$$\int_{-\infty}^{+\infty} |\psi(t)|^2 dt < \infty \tag{15}$$

The first equation sets a zero-mean condition on the mother wavelet while the second one indicates it has finite energy. The mother wavelet is scaled and shifted giving new wavelets which will be used to correlate the signal to analyze [46, 47]:

$$C_{u,s} = \int_{-\infty}^{+\infty} f(t)\psi^*_{u,s}(t)dt \tag{16}$$

where

$$\psi_{u,s}(t) = \frac{1}{\sqrt{s}}\psi(\frac{t-u}{s}) \tag{17}$$

The coefficients $C_{u,s}$ are the results of a continuous wavelet transform (CWT). However, the CWT implies an infinite number of dilatation and translation operations, which makes it almost impractical in reality. Hence, there was a need for a method to use a reduced number of dilatation and translation operations, while being able to obtain a good reconstruction of the original signal. In 1989, Mallat proposed an algorithm that implements a fast discrete wavelet transform by using a combination of high and low-pass filters [48]. This technique is also known as sub-band coding in the signal processing community. Figure 2 describes how the algorithm was designed.

Mallat's algorithm provides a signal representation in terms of the decomposition coefficients. These coefficients can be then manipulated to process the signal. Wavelet denoising is a signal operation consisting of applying a threshold on each signal coefficient [40, 49]. The threshold T is based on the 1st-level detail signal d_1 and was calculated as follows [43]:

$$T = \frac{med(|d1|)\sqrt{2\log n}}{0.6745}$$

where *med* is the median function and n is the length of the signal. The idea is that the coefficients associated with noise are below the threshold value, while the coefficients associated with the signal are above the threshold value. Thus wavelet denoising is a more powerful tool compared to the classical low-pass filtering (e.g. using a Butterworth filter) as it enables to remove noise from the whole frequency spectrum.

2.3. Feature extraction

After the pre-processing stage, statistical, frequency and time-frequency features were extracted from the acceleration signals.

2.3.1. Time and stride interval related features

A general form of signal can be defined as $X = \{x_1, x_2, \ldots, x_n\}$. Then, the following parameters can be extracted [50]:

- The standard deviation which characterizes the variability of signals was defined as follows:

$$\sigma_X = \sqrt{\frac{1}{n-1}\sum_{i=1}^{n}(x_i - \mu_X)^2} \tag{18}$$

  with μ_X being the mean of the signal.

- The skewness which characterizes the asymmetry of signals was defined as follows:

$$\xi_X = \frac{\frac{1}{n}\sum_{i=1}^{n}(x_i - \mu_X)^3}{(\frac{1}{n}\sum_{i=1}^{n}(x_i - \mu_X)^2)^{\frac{3}{2}}} \tag{19}$$

- The kurtosis which characterizes the behavior of extreme data points was defined as follows:

$$\gamma_X = \frac{\frac{1}{n}\sum_{i=1}^{n}(x_i - \mu_X)^4}{(\frac{1}{n}\sum_{i=1}^{n}(x_i - \mu_X)^2)^2} \tag{20}$$

- The cross-correlation coefficient at the zeroth lag of two signals $X = \{x_1, x_2, \ldots, x_n\}$ and $Y = \{y_1, y_2, \ldots, y_n\}$ defined as follows:

$$\eta_{X,Y} = \frac{\sum_{i=1}^{n}(x_i - \mu_X)(y_i - \mu_Y)}{\sqrt{\sum_{i=1}^{n}(x_i - \mu_X)^2}\sqrt{\sum_{i=1}^{n}(y_i - \mu_Y)^2}} \tag{21}$$

  with μ_X and μ_Y being the mean of signals X and Y.

Finally, calculating harmonic ratios is a way to assess smoothness of walking [51], [52]. Therefore we computed the harmonic ratios of low-pass filtered acceleration signals in every anatomical direction for each stride. The cutoff frequency of the filter was set to 30 Hz. First the discrete Fourier transform was calculated:

$$a_{stride} = \sum_{n=0}^{N-1} C_n \sin(n\omega_0 t + \phi_n) \tag{22}$$

where C_n is the harmonic coefficient, ω_0 is the stride frequency and ϕ_n is the phase. We then summed the first 20 harmonic coefficients to compute the harmonic ratios. The latter are defined as follows:

$$HR_{\text{AP and V}} = \left\langle \frac{\sum_{n=2,4,6,\ldots}^{20} C_n}{\sum_{n=1,3,5,\ldots}^{20} C_n} \right\rangle \tag{23}$$

$$HR_{\text{ML}} = \left\langle \frac{\sum_{n=1,3,5,\ldots}^{20} C_n}{\sum_{n=2,4,6,\ldots}^{20} C_n} \right\rangle \tag{24}$$

where $\langle \sum C_n / \sum C_n \rangle$ is the average ratio over all strides.

2.3.2. Frequency features

The following characteristics were identified in the frequency domain [53]:

- The peak frequency defined by:

$$f_p = \underset{f \in [0, f_{max}]}{\arg\max} |F_X(f)|^2 \tag{25}$$

  where $F_X(f)$ is the Fourier transform of the signal and f_{max} is the sampling frequency (100 Hz in this experiment)

- The spectral centroid defined by:

$$f_c = \frac{\int_0^{f_{max}} f|F_x(f)|^2 df}{\int_0^{f_{max}} |F_X(f)|^2 df} \tag{26}$$

- The bandwidth defined by:

$$BW = \sqrt{\frac{\int_0^{f_{max}} (f - f_c)|F_X(f)|^2 df}{\int_0^{f_{max}} |F_X(f)|^2 df}} \tag{27}$$

2.3.3. Time-frequency features

We also took into account features in the time-frequency domain. A 10-level discrete wavelet transform was applied using discrete Meyer's wavelet [54]. The decomposition can be written as $W_X = [a_{10}\ d_{10}\ d_9 \dots d_1]$ where a_{10} is the approximation signal and d_k is the k^{th}-level detail signal.

- The relative energy in each wavelet decomposition level was computed as follows:
  The expression of the approximation signal energy is

$$E_{a_{10}} = \|a_{10}\|^2 \tag{28}$$

  $\|\bullet\|$ being the Euclidean norm.

  The k^{th}-level detail signal energy is expressed as follows:

$$E_{d_k} = \|d_k\|^2 \tag{29}$$

  The total energy in the signal is:

$$E_T = a_{10} + \sum_{k=1}^{10} E_{d_k} \tag{30}$$

  Finally the relative energy in each decomposition level is:

$$\Phi_a = \frac{E_{a_{10}}}{E_T} \times 100\% \tag{31}$$

$$\Phi_d = \frac{E_{d_k}}{E_T} \times 100\% \tag{32}$$

- Using the previously computed wavelet energy features, the wavelet entropy was calculated as follows:

$$\Theta_X = -\Phi_{a_{10}} \log_2 \Phi_{a_{10}} - \sum_{k=1}^{10} \Phi_{d_k} \log_2 \Phi d_k \tag{33}$$

2.4. Data analysis

In order to identify differences between participant groups and processing methods, we fit a series of linear mixed models with each extracted feature as the dependent variable; participant group, processing method and their interaction as fixed effects of interest; and a participant random effect to account for multiple measurements from the same participants and resulting stochastic non-independence of observations.

We used appropriately constructed means contrasts to compare processing methods within each participant group, compare participant groups under each processing method, and compare participant group differences across processing methods. To compare anatomical directions, we first computed three anatomical direction differences in each of the extracted feature. Next we fitted a similar linear mixed model with each of the anatomical direction differences as the dependent variable; participant group, processing method and their interaction as fixed effects of interest; and a participant random effect. We used least squares means to estimate anatomical direction differences within each participant group and processing method combination. The significance level α was set to 0.05.

SAS version 9.3 (SAS Institute, Inc., Cary, North Carolina) was used for all statistical analyses.

3. Results

The results of our analysis are summarized hereafter. Features are analyzed for each pre-proccesing operation and are compared to the original data.

3.1. Time and stride interval related features

Tables 1 and 2 summarize the differences found for the time domain features.

3.1.1. Original data

Group differences. We did not observe any differences between groups in any directions when considering the variability of signals σ ($p > 0.10$). When considering the skewness of signals, we found no statistical differences between groups along every direction ($p > 0.09$). Kurtosis values did not differ significantly for any group ($p > 0.29$) neither. Finally, we found that $\eta_{ML,V}$ values were different between PD and PN subjects ($p < 0.02$). HC subjects also had greater harmonic ratios than PD subjects along every anatomical direction ($p < 0.03$).

Anatomical directions differences. Variability of signals statistically differed between anatomical directions for each group ($p < 0.01$). When we examined skewness of signals we found differences between every anatomical direction for each group ($p \ll 0.01$) except between ξ_{ML} and ξ_{AP} for PD subjects ($p > 0.26$). For HC patients, the behavior of extreme points was different between the ML and V directions ($p < 0.02$). Also, differences between $\eta_{ML,V}$ and $\eta_{V,AP}$ as well as between $\eta_{ML,AP}$ and $\eta_{V,AP}$ were identified for HC and PN subjects ($p \ll 0.01$). Each group had higher harmonic ratios in the V direction than in the ML direction ($p \ll 0.01$). Moreover, HCs and PNs had greater ratios in the AP direction than in the ML direction ($p \ll 0.01$). Finally, PN patients had a greater ratio in the V direction rather than in the AP direction ($p < 0.02$).

3.1.2. Corrected data

Group differences. As shown in Figure 3, the correction shifted the signals to zero mean. The variability and kurtosis of signals followed the same trend as the uncorrected signals. Few changes between original and corrected data were noticed when analyzing asymmetry of signals (ξ feature). A difference between HC and PN participants was present in the corrected data along the ML axis ($p < 0.01$). Lastly, for $\eta_{ML,V}$ we did not find differences between PD and PN ($p > 0.92$). We also found that HCs had higher harmonic ratios than PNs in the AP direction ($p < 0.04$). Moreover the ratio along the V-axis was found higher for PNs than for PDs ($p < 0.04$).

Anatomical directions differences. The standard deviations of signals in the ML and AP directions were not different for PN and PD groups after correction ($p > 0.14$). We examined skewness of signals but did not find differences between the ML and AP directions for PN subjects ($p > 0.73$) anymore. The comparison of $\eta_{ML,V}$ and $\eta_{ML,AP}$ lead to no significant difference ($p > 0.68$). Lastly, the statistical difference for harmonic ratios between ML and AP disappeared for PN participants ($p > 0.15$). A new significant difference for HC controls and PD subjects was noticed: the ratio in the vertical direction was higher than in the anterior-posterior direction ($p < 0.01$).

3.1.3. Denoised data

Group differences. When considering the statistical features, we noticed a difference in standard deviations between HC and PD participants along the AP direction ($p < 0.05$) compared to the raw data. Skewness, kurtosis and cross-correlations followed the same trend as for the raw signals. For harmonic ratios, we found no difference between HC subjects and PD ones ($p > 0.10$) along the ML direction.

Anatomical directions differences. No changes in values for standard deviation, skewness and cross-correlation, and harmonic ratios could be noticed after denoising. The kurtosis difference between the ML and V directions did not appear anymore for HC patients ($p > 0.14$). For the PN group, γ_{AP} was different from γ_{ML} ($p < 0.05$).

3.1.4. Corrected and denoised data

Groups differences. Skewness values were different between HCs and PNs ($p < 0.01$) along the ML-axis and between HCs and PDs along the AP-axis ($p < 0.05$). PD and PN groups were not significantly different for $\eta_{ML,V}$ values ($p > 0.70$). Harmonic ratios were not statistically different between HCs and PDs along the ML-axis ($p > 0.1$). We also found that HC controls had greater harmonic ratios than PN subjects in the AP direction ($p < 0.03$). Moreover, PNs had a greater harmonic ratio than PDs in the vertical direction ($p < 0.05$).

Anatomical directions differences. Our results showed that standard deviations were not statistically different in in the ML/AP directions for PN ($p > 0.56$) nor for PD groups ($p > 0.45$). No difference was observed for PN subjects when comparing ξ_{ML} and ξ_{AP} ($p > 0.81$). The kurtosis of signals measured in all three directions were different for PNs ($p < 0.03$) and PD subjects ($p < 0.05$). No difference in kurtosis values could be observed between the V and ML directions for HC patients ($p > 0.24$). Finally for PD patients, $\eta_{ML,V}$ and $\eta_{V,AP}$ were not statistically different ($p > 0.43$). Harmonic ratios were not different between the ML and AP directions for PNs ($p > 0.51$). We also observed that HC and PD subjects had a greater harmonic ratio in the vertical direction than in the anterior-posterior one ($p < 0.02$).

3.1.5. Denoised and corrected data

Group differences. The results were almost identical to the results obtained when performing tilt correction followed by denoising, except that skewness of signals measured along the ML-axis was different between HC and PN groups ($p < 0.01$).

Anatomical direction differences. Similar results to tilt correction followed by denoising were obtained for this preprocessing step. However, no statistical differences between the values of $\eta_{ML,V}$ and $\eta_{ML,AP}$ were observed for PD subjects.

3.2. Frequency features

Tables 3 and 4 summarize the differences found for the frequency domain features.

3.2.1. Original data

Group differences. No statistical differences for the peak frequencies were observed between groups ($p > 0.10$). The spectral centroids exhibited differences between HC and PD subjects for signals acquired along the AP-axis ($p < 0.03$). We finally noticed that signals measured on HC and PD subjects had different bandwidths in the ML and AP directions ($p < 0.03$).

Anatomical direction differences. When we analyzed peak frequencies, we observed statistical differences for PNs and PDs between the ML and V directions and between the ML and AP directions ($p < 0.02$). The spectral centroids were statistically different between the ML and V directions for all groups ($p < 0.02$) and between the V and AP directions for PN and PD groups ($p \ll 0.01$). Finally, we observed differences for all groups between bandwidths of signals acquired along the V and AP directions ($p \ll 0.01$) as well as between the ML and V directions ($p \ll 0.01$).

3.2.2. Corrected data

Group differences. In the ML direction we found that signals retrieved from HC subjects had greater peak frequencies than PD ($p < 0.02$) and PN ($p < 0.03$) patients. For spectral centroids, we observed a difference between PN and HC groups ($p < 0.04$) when looking at f_{cAP}. Lastly, BW_{AP} values were different for PN and HC volunteers ($p < 0.04$).

Anatomical direction differences. HC subjects had different spectral centroids when we compared signals along the AP-axis and V-axis ($p < 0.03$). For PNs, we also found that f_{cAP} was greater than f_{cML} ($p < 0.03$). Differences between bandwidths of signals in the AP and ML directions were found for PN ($p < 0.03$) and PD groups ($p < 0.05$).

Anatomical direction differences. After denoising signals, we did not observe differences for any group between the ML and V directions when we analyzed spectral centroids ($p > 0.05$). However, we observed different centroid values between signals in the AP and ML directions for PN subjects ($p < 0.04$). Bandwidths for signals along the ML and V directions were not statistically different for HCs ($p > 0.06$). Signals from PN subjects had different bandwidth values in the AP and ML directions ($p < 0.04$).

3.2.3. Corrected and denoised

Group differences. When comparing centroids for the corrected-denoised data and the raw data, we found that spectral centroids were different between PN and HC groups for signals measured in the AP direction ($p < 0.05$). The same trend could be observed for the bandwidth of these signals ($p < 0.01$).

Anatomical direction differences. We noticed that spectral centroids f_{cML} did not differ significantly from f_{cV} for PN ($p > 0.49$) and PD subjects ($p > 0.05$) after pre-processing signals. However, statistical differences between the ML and AP directions were observed for PN subjects only ($p < 0.02$). Bandwidths of signals in the AP and ML directions were different for PN and PD subjects ($p < 0.01$).

3.2.4. Denoised and corrected data

Group differences. The same results were obtained as for performing tilt correction followed by denoising.

Anatomical direction differences. Significant differences were observed between peak frequencies of signals in the V and AP directions for PN subjects ($p \ll 0.01$). Otherwise the same trend as the corrected-denoised data was observed.

3.2.5. Denoised data

Group differences. No differences for $f_{c_{AP}}$ were found between HC and PD groups after denoising signals ($p > 0.05$). PN and HC groups had different bandwidths along the AP-axis ($p < 0.02$).

3.3. Time-frequency features

The four last detail level coefficients held nearly no energy. Thus, we did not consider these levels any further. Denoising did not affect the energy in the time-frequency bands. However applying correction changed the repartition of the energy. Indeed in the vertical direction the energy of the approximation signal decreased whereas the one in the 10^{th} to the 5^{th} detail signal increased. Depending on the decomposed signal studied differences between groups and anatomical directions were also observed. When both pre-processing operations were applied we could observe similar results to the ones we observed when applying correction only.

3.3.1. Original data

Group differences. We did not observe significant groups differences in any time-frequency band for accelerations measured along the medio-lateral axis ($p > 0.06$). More than 99% of the energy of the V acceleration signals was concentrated in the approximation level. We discarded the rest of the coefficients in the V direction as the detail signals contained insignificant amounts of energy. However, no group differences could be seen along this axis ($p > 0.98$) or the AP axis ($p > 0.40$). No group differences were observed for the wavelet entropy of signals ($p > 0.17$).

Anatomical direction differences. For all groups, the a_{10} coefficients from the V direction contained higher energy than the same coefficients in the ML ($p \ll 0.01$) and AP direction ($p < 0.04$). Also, HCs had higher energy contained in a_{10} coefficients in the AP direction than in the ML direction ($p < 0.04$). d_8 coefficients contained higher energy in the ML direction than in the V direction for all groups ($p < 0.04$) and in comparison to the AP direction for the HC group ($p \ll 0.01$). Signals from PD subjects had higher energy in the AP direction compared to the signals in the V direction ($p < 0.04$). In the 7^{th} decomposition level, the energy was higher for signals retrieved along the ML-axis compared to those along the V direction ($p \ll 0.01$) and the AP direction ($p < 0.03$) for HC subjects. However no difference was noticed when we compared the signals in the V and AP directions ($p > 0.08$). In any direction, no differences were noticed for the other groups ($p > 0.2$). We noticed that the energy was lower for d_6 signals along the V-axis compared to those along the AP-axis for HCs ($p < 0.01$). For all groups, the energy in d_5 signals was higher along the ML-axis than the V-axis ($p < 0.04$). For PD subjects, we noticed that signals in the ML direction had higher

energy compared to the AP direction ($p < 0.05$). We did not observed any difference when we compared signals in the V and AP directions ($p > 0.22$).

Interestingly we noticed that for each group the entropy values in the V direction were close to 0 while they were higher in the other directions ($p \ll 0.01$). We also noticed that Θ_{ML} was higher than Θ_{AP} for HCs ($p < 0.01$) and PD subjects ($p < 0.02$), while we observed no difference for PN subjects ($p > 0.1$).

3.3.2. Corrected data

Group differences. After the correction step, we noticed that the energy in wavelet decomposition levels was repartitioned for every group in every direction. HCs had higher energy than PD subjects along the ML-axis in the d_7 signal ($p \ll 0.01$). The same results were obtained for HCs and PNs when we analyzed the d_7 ($p < 0.02$) and d_5 ($p < 0.05$) detail signals along the same direction. In the V direction, while most of the energy was concentrated in the approximation signal for the raw data, the energy in the approximation signal after correction diminished and increased in the first 6 detail signals $\Phi_{V_{d_{10}}}, \Phi_{V_{d_9}}, \ldots, \Phi_{V_{d_5}}$ ($p \ll 0.01$). However, we did not notice any group differences along the V-axis. Statistical differences along the AP-axis were observed in the d_7 signals between HC and PD/PN subjects ($p < 0.02$) and in the d_6 detail signals between HCs and PNs ($p < 0.05$).

Overall the entropy in the V direction was lower than in the other directions. However for PN and PD subjects it was not statistically different from the entropy in the ML direction ($p > 0.19$) and from the entropy in the AP direction for PN patients ($p > 0.06$). Finally Θ_{ML} and Θ_{AP} were not statistically different for any group ($p > 0.28$).

Anatomical direction differences. After correction there were no significant differences between a_{10} signals in the V and ML direction and signals in the V and AP directions for all groups ($p > 0.05$). However, we observed that signals from PDs had higher energy in the ML direction than the AP direction ($p < 0.04$). The energy in the d_8 signals was not distinguishable between the ML and V directions for PDs ($p > 0.26$) and PNs ($p > 0.44$). For PDs, we were unable to distinguish between the V and AP directions ($p > 0.59$). HCs had no statistical differences in d_7 signals between ML and V/AP directions ($p > 0.09$). PDs had higher energy for the signals along the V-axis than for signals along the ML-axis ($p < 0.05$). We also observed that signals for all three groups in the 6^{th} decomposition level had higher energy in the V direction than in the ML direction ($p \ll 0.01$). The same results were obtain when we compared signals in the AP and ML directions ($p \ll 0.01$). For HCs in particular, there were no difference between signals in the V and AP directions ($p > 0.45$). For PN subjects, energy in the V direction was higher than in the AP direction ($p \ll 0.01$). Finally the energy was higher in d_5 signals in the ML direction than in the AP direction for PN

patients ($p \ll 0.01$) but we were unable to distinguish between signals in the ML and V directions for HCs and PDs ($p > 0.14$) nor between signals in the ML and AP directions for PD subjects ($p > 0.29$).

We found no significant difference between Θ_{ML} and Θ_V for PD and PN subjects after correction ($p > 0.19$), nor between Θ_{ML} and Θ_{AP} for HC and PD subjects ($p > 0.28$) nor between Θ_{AP} and Θ_V for PN subjects ($p > 0.06$).

3.3.3. Denoised data

Group differences. The energy repartition for denoised data was similar to the original signal. We still had more than 99% of the energy concentrated in the approximation signal $\Phi_{Va_{10}}$. The energy and the entropy of the signals followed the same trend as the original ones.

Anatomical direction differences. When we analyzed the a_{10} signals there was no significantly different energy between signals in the V and AP directions for PD and PN subjects ($p > 0.05$). For healthy subjects we were not able to distinguish between signals in the AP and the ML directions ($p > 0.06$). Similarly for PD subjects, we were not able to distinguish between signals along the V-axis and the ML-axis ($p > 0.05$). The signals in the 8^{th} decomposition level followed the same trend as the corresponding corrected signals while d_7 and d_6 signals followed the same same trend as the corresponding raw signals. Lastly we analyzed d_5 signals and we noticed for PNs that energy was higher in signals in the ML direction compared to accelerations in the AP direction ($p < 0.04$). This was not case however for PD patients ($p > 0.07$).

The entropy of signals in the ML direction was not significantly different from the one of signals in the AP direction for the PD group ($p > 0.25$). Otherwise the entropy of denoised signals followed the same trend as the raw signals.

3.3.4. Corrected and denoised data

Groups differences. Similarly to the corrected signals the repartition of the energy was different. In the ML direction, the energy in the approximation signal a_{10} was higher for PD subjects than for HC ones ($p < 0.04$). On the contrary, there was more energy in the d_7 ($p \ll 0.01$) and d_6 ($p < 0.04$) signals for healthy controls than for PD patients. The energy in the d_8 ($p < 0.04$) and d_7 ($p \ll 0.01$) signals was also higher for healthy controls than for PN subjects. Still along the ML-axis, PN patients had higher energy than HCs in the d_5 signal ($p < 0.02$). In the V direction the relative energy of the d_6 signal was lower for PDs than for PNs ($p < 0.01$). In the d_5 signal the opposite was observed ($p < 0.01$). In the AP direction the energy in the d_7 and d_6 signals was higher for the HC group than for the PD ($p < 0.04$) and PN groups ($p < 0.02$). Also, the energy in the d_5 signal was higher for PD subjects compared to PNs ($p < 0.03$).

No difference between groups were observed when we analyzed entropies in every direction ($p > 0.18$). We did not observed differences between anatomical directions neither for PDs and PNs ($p > 0.15$). Only signals from healthy controls had a larger entropy along the ML-axis ($p < 0.05$) and AP-axis ($p < 0.04$) compared to the V-axis.

Anatomical direction differences. The energy in the a_{10} signals was similar to the energy in signals after correction. However for PN subjects, we observed that signals in the V direction contained less energy than signals in the ML direction ($p < 0.04$). For the same group of subjects, the energy along the V-axis was also lower than energy in signals along the AP-axis ($p < 0.05$). In the d_7 signals PD subjects had higher energy in the V direction than in the ML ($p < 0.03$) and AP directions ($p < 0.04$). Results for the d_8, d_6 and d_5 signals were the same as the corresponding signals after the correction step. The same trend as for corrected signals was observed when we examined the wavelet entropy differences, except that Θ_{AP} and Θ_V were not statistically different for PDs ($p > 0.15$).

3.3.5. Denoised and corrected data

Group differences. The results were very similar to the ones we found in the previous step. Energy in signals from PD subjects was higher than in signals measured on HCs in the V direction ($p < 0.05$).

Anatomical direction differences. The same trend was observed compared to accelerations in the previous step except that we did not observe a significant difference of energy between signals in the AP and V directions for PN subjects in the a_{10} approximation signal ($p > 0.05$) nor for PD subjects in the d_7 detail signal ($p > 0.07$). The entropy after the denoised-corrected step followed the same trend as the previous step.

4. Discussion

The major impact of this work is on the analysis of gait accelerometry signals. Our results conclusively show that pre-processing operations such as tilt correction can yield additional discrimination amongst patient groups, while other pre-processing operations such as wavelet denoising have no impacts on discriminatory patterns observed in gait accelerometry signals. Our findings therefore imply it is beneficial to pre-process gait accelerometry signals, but also imply that during a gait assessment procedure, accelerometers do not need to be positioned perfectly perpendicular to the walking surface, as the tilt correction procedure can be used to remove the tilt effects without detrimental effects on the analysis results.

We successfully extracted features in time, frequency, time-frequency domains. In the time domain, by applying the tilt correction, we were able to distinguish between healthy controls and subjects with

Parkinson's disease and peripheral neuropathy. Specifically, we observed greater skewness for subjects suffering from peripheral neuropathy than for healthy controls in the medio-lateral direction. Nevertheless, no difference between participants having Parkinson's disease and peripheral neuropathy could be observed using this feature. Concerning harmonic ratios, using the original data the only group differences found were between healthy controls and persons with Parkinson's disease, where controls exhibited greater walking symmetry in all directions of motion. The tilt correction led to further discrimination between the groups and showed that participants with peripheral neuropathy had a greater symmetry than those with Parkinson's disease, whereas healthy controls had a greater symmetry than subjects with peripheral neuropathy. Also the tilt correction showed that every group had a harmonic ratio higher in the vertical than in the anterior-posterior direction.

In the frequency domain and after tilt correction was applied, peak frequencies in the medio-lateral direction and the spectral centroids in the anterio-posterior direction allowed to distinguish between controls and clinical groups. Also, the bandwidth of signals for subjects with peripheral neuropathy was greater than for healthy control in the anterior-posterior direction after applying tilt correction.

Time-frequency features were the most difficult to analyze. An obvious observation is that the application of tilt correction changed the energy repartition for every group especially in the vertical direction. The energy was transferred from the approximation signal representing low frequencies to the six first detail signals representing higher frequencies. However it was difficult to distinguish between groups using the features in this domain.

Denoising had practically no effect on the calculated characteristics since, as shown on Figure 3, the signals had a low level of noise. Finally, when applying both correction and denoising we observed that the results were most of the time the accumulation of the results found when we applied the preprocesses separately.

We believe that tilt correction should be applied to gait accelerometry signals regardless of one's intends to analyze gait accelerometry axes independently, as in this manuscript, or jointly through a resultant vector. With no tilt corrections, the resultant vector denoting walking acceleration would point to an incorrect direction, even if the three anatomical axes are analyzed jointly.

The presented results open up a potential research area dealing with the gait assessment using smart phones. We believe that our results are applicable in those cases as well, as long as smart phones are affixed to a human body in order to avoid non-motion related acceleration components.

Additional features can be extracted if accelerometers are attached to legs/ankles. These additional features can be very advantageous for machine learning applications, which aim to differentiate gait among different pathological groups. However, it may be difficult to relate every feature to a clinical outcome.

In these cases, advanced machine learning approaches such as neural networks and artificial intelligence algorithms are suitable to relate a group of features to specific clinical outcomes. These machine learning algorithms can be also used to differentiate between patient groups if needed.

5. Conclusion

As accelerometry becomes more widely used to assess age- and disease-related differences in the motor control of walking and changes in gait control with rehabilitation, it is critical that researchers adopt similar methods of pre-processing acceleration data. This will allow for valid comparisons of findings across studies. In this paper, we pre-processed gait accelerometry signals using different techniques in order to understand the impact on the extracted signal features in time, frequency and time-frequency domains. Specifically, we examined the effects of tilt correction and denoising as well as their combined effects. Our data indicate that denoising had minimal or no effect on extracted signal features while tilt correction yielded additional discrimination between healthy and clinical groups. Hence, while denoising may not be necessary for pre-processing of the acceleration signals, tilt correction is recommended as an important component of their pre-processing. Future studies should therefore consider pre-processing gait accelerometry signals before extracting any features.

6. Acknowledgements

This work was supported in part by the Pittsburgh Claude D. Pepper Older Americans Independence Center (NIA P30 AG 024827).

References

[1] D. Winter, Human balance and posture control during standing and walking, Gait and Posture 3 (1995) 193–214.

[2] J. D. Schaafsma, N. Giladi, Y. Balach, A. L. Bartels, T. Gurevich, J. M. Hausdorff, Gait dynamics in parkinson's disease: relationship to parkinsonian features, falls and response to levodopa, Journal of the Neurological Sciences 212 (2003) 47–53.

[3] H. B. Menz, S. R. Lord, R. C. Fitzpatrick, Acceleration patterns of the head and pelvis when walking on level and irregular surfaces, Gait and Posture 18 (2003) 35–46.

[4] R. Rozendal, Clinical gait analysis: Problems and solutions?, Human Movement Science 10 (1991) 555–564.

[5] M. W. Whittle, Clinical gait analysis: A review, Human Movement Science 15 (1996) 369–387.

[6] J. S. Brach, J. E. Berlin, J. M. VanSwearing, A. B. Newman, S. A. Studenski, Too much or too little step width variability is associated with a fall history in older persons who walk at or near normal gait speed, Journal of NeuroEngineering and Rehabilitation 2 (2005) 21.

[7] M. Jylhä, J. M. Guralnik, J. Balfour, L. P. Fried, Walking difficulty, walking speed,, Journal of Gerontology 56A (2001) 609–617.

[8] S. Marquis, M. M. Moore, G. S. Diane B. Howieson, H. Payami, J. Kaye, R. Camicoli, Independant predictors of cognitive decline in healthy elderly persons, Arch. Neurol. 59 (2002) 601–606.

[9] T. L. Hayes, F. Abendroth, A. Adami, M. Pavel, T. A. Zitzelberger, J. A. Kaye, Unobtrusive assessment of activity patterns associated with mild cognitive impairment, Alzheimer's & Dementia 4 (2008) 395–405.

[10] S. Studenski, S. Perera, K. Patel, C. Rosano, K. Faulkner, M. Inzitari, J. Brach, J. Chandler, P. Cawton, E. B. Connor, M. Nevitt, M. Visser, S. Kritchevsky, S. Badinelli, T. Harris, A. B. Newman, J. Cauley, L. Ferrucci, J. Guralnik, Gait speed and survival in older adults, Journal of the American Medical Association 305 (2011) 50–58.

[11] J. Kaye, N. Mattek, H. Dodge, T. Burachio, D. Austin, S. Hagler, M. Pavel, T. Hayes, One walk a year to 1000 within a year: Continuous in-home unobtrusive gait assessment of older adults, Gait and Posture 35 (2011) 197–202.

[12] H. G. Kang, J. B. Dingwell, A direct comparison of local dynamic stability during unperturbed standing and walking, Experimental Brain Research 172 (2006) 35–48.

[13] M. S. Redfern, J. DiPasquale, Biomechanics of descending ramps, Gait and Posture 6 (1997) 119–125.

[14] R. Moe Nilssen, A new method for evaluating motor control in gait under real-life environmental conditions. Part 1: The instrument, Clinical Biomechanics 13 (1998) 320–327.

[15] R. Moe-Nilssen, J. L. Helbostad, Trunk accelerometry as a measure of balance control during quiet-standing, Gait and Posture 16 (2002) 60–68.

[16] E. Sejdić, B. Findlay, C. Merey, T. Chau, The effects of listening to music or viewing television on human gait, Computers in Biology and Medicine 43 (10) (2013) 1497–1501.

[17] R. E. Mayagoitia, J. C. Lötters, P. H. Veltink, H. Hermens, Standing ealance evaluation using a triaxial acceleroemeter, Gait and Posture 16 (2002) 55–59.

[18] M. D. Chang, E. Sejdić, V. Wright, T. Chau, Measures of dynamic stability: Detecting differences between walking overground and on a compliant surface, Human Movement Science 29 (6) (2010) 977–986.

[19] K. A. Lowry, N. Lokenvitz, A. L. Smiley-Oyen, Age- and speed-related differences in harmonic ratios during walking, Gait and Posture 35 (2) (2012) 272–276.

[20] F. Riva, M. C. Bisi, R. Stagni, Gait variability and stability measures: Minimum number of strides and within-session reliability, Computers in Biology and Medicine 50 (2014) 9–13.

[21] A. Hartmann, K. Murer, R. A. de Bie, E. D. de Bruin, Reproducibility of spatio-temporal gait parameters under different conditions in older adults using a trunk tri-axial accelerometer system, Gait and Posture 30 (3) (2009) 351–355.

[22] J. Wikstrom, G. Georgoulas, T. Moutsopoulos, A. Seferiadis, Intelligent data analysis of instrumented gait data in stroke patients - a systematic review, Computers in Biology and Medicine 51 (2014) 61–72.

[23] M.-J. Gu, A. B. Schultz, N. T. Shepard, N. B. Alexander, Postural control in young and elderly adults when stance is perturbed, Journal of Biomechanics 29 (1996) 319–329.

[24] K. Tong, M. H. Granat, A practical gait analysis system using gyroscopes, Medical Engineering and Physics 21 (1999) 87–94.

[25] I. P. I. Pappas, T. Keller, S. Mangold, M. R. Popovic, V. Dietz, M. Morari, A reliable gyroscope based gait phase detection sensor embedded in a shoe insole, IEEE Sensors Journal 4 (2004) 268–274.

[26] W. Tao, T. Liu, R. Zheng, H. Feng, Gait analysis using wearable sensors, Sensors 12 (2012) 2255–2283.

[27] J. J. Kavanagh, H. B. Menz, Accelerometry: A technique for quantifying movement patterns during walking, Gait and Posture 28 (2008) 1–15.

[28] G.-A. Hansson, P. Asterland, N.-G. Holmer, S. Skerfving, Validity and reliability of triaxial accelerometers for inclinometry in posture analysis, Medical and Biological Engineering and Computing 39 (2001) 405–413.

[29] H. J. Yack, R. C. Berger, Dynamic stability in the elderly: identifying a possible measure, Journal of Gerontology 48 (5) (1993) M225–M230.

[30] J. J. Kavanagh, R. S. Barrett, S. Morrison, Upper body accelerations during walking in healthy young and elderly men, Gait and Posture 20 (3) (2004) 291–298.

[31] E. Sejdić, K. A. Lowry, J. Bellanca, M. S. Redfern, J. S. Brach, A comprehensive assessment of gait accelerometry signals in time, frequency and time-frequency domains, IEEE Transactions on Neural Systems and Rehabilitation Engineering 22 (3) (2014) 603–612.

[32] R. Soangra, T. E. Lockhart, N. Van de Berge, An approach for identifying gait events using wavelet denoising technique and single wireless imu, Proceedings of the Human Factors and Ergonomics Society Annual Meeting 55 (1) (2011) 1990–1994.

[33] R. Soangra, T. E. Lockhart, J. Lach, E. M. Abdel-Rahman, Effects of hemodialysis therapy on sit-to-walk characteristics in end stage renal disease patients, Annals of Biomedical Engineering 41 (4) (2013) 795–805.

[34] J. J. Kavanagh, S. Morrison, D. A. James, R. Barrett, Reliability of segmental accelerations measured using a new wireless gait analysis system, Journal of Biomechanics 39 (15) (2006) 2863–2872.

[35] A. Dalton, H. Khalil, M. Busse, A. Rosser, R. van Deursen, G. OLaighin, Analysis of gait and balance through a single triaxial accelerometer in presymptomatic and symptomatic Huntington's disease, Gait and Posture 37 (1) (2013) 49–54.

[36] M. Schenkman, M. Morey, M. Kuchibhatla, Spinal flexibility and balance control among community-dwelling adults with and without Parkinson's disease, Journal of Gerontology: Medical Sciences 55A (8) (2000) M441–M445.

[37] J. K. Richardson, S. B. Thies, T. K. Demott, J. A. Ashton-Miller, A comparison of gait characteristics between older women with and without peripheral neuropathy in standard and challenging environments, Journal of the American Geriatrics Society 52 (9) (2004) 1532–1537.

[38] K. Jordan, J. H. Challis, K. M. Newell, Walking speed influences on gait cycle variability, Gait and Posture 26 (1) (2007) 128–134. doi:10.1016/j.gaitpost.2006.08.010.

[39] G. L. Smidt, J. S. Arora, R. C. Johnston, Accelerographic analysis of several types of walking, American Journal of Physical Medicine 50 (1971) 285–300.

[40] D. L. Donoho, De-noising by soft-thresholding, IEEE Transactions on Information Theory 41 (1995) 613–627.

[41] S. Stanković, I. Orović, E. Sejdić, Multimedia Signals and Systems, Springer US, New York, NY, 2012.

[42] E. Sejdić, I. Djurović, J. Jiang, Time-frequency feature representation using energy concentration: An overview of recent advances, Digital Signal Processing 19 (1) (2009) 153–183.

[43] J. Lee, E. Sejdić, C. M. Steele, T. Chau, Effects of liquid stimuli on dual-axis swallowing accelerometry signals in a healthy population, BioMedical Engineering OnLine 9 (2010) 7.

[44] O. A. Rosso, S. Blanco, J. Yordanova, V. Kolev, A. Figiola, M. Schürmann, E. Basar, Wavelet entropy: a new tool for analysis of short duration brain electric signals, Journal of Neuroscience Methods 105 (2001) 65–75.

[45] M. N. Nyan, F. Tay, K. Seah, Y. Sitoh, Classification of gait patterns in the time-frequency domain, Journal of Biomechanics 39 (2005) 2647–2656.

[46] S. Mallat, A Wavelet tour of signal processing (2nd edition), Academic Press, 1999.

[47] A. N. Akansu, M. V. Tazebay, M. J. Medley, P. K. Das, Wavelet and subband transforms: Fundamentals and communication applications, IEEE Communications Magazine (1997) 104–115.

[48] S. G. Mallat, A theory for multiresolution signal decomposition: The wavelet representation, IEEE Transactions on Pattern Analysis and Machine Intelligence 11 (1989) 674–693.

[49] D. L. Donoho, I. M. Johnston, Adapting to unknown smoothness via wavelet shrinkage, Journal of the American Statistical Association 90 (1995) 1200–1224.

[50] A. Papoulis, Probability, Random Variables, and Stochastic Processes, 3rd Edition, New York: WCB/McGraw-Hill, 1991.

[51] J. S. Brach, D. McGurl, D. Wert, J. M. VanSwearingen, S. Perera, R. Cham, S. Studenski, Validation of a measure of smoothness of walking, Journal of Gerontology 66A (2011) 136–141.

[52] J. Bellanca, K. Lowry, J. VanSwearingen, J. Bach, M. Redfern, Harmonic ratios: A quantification of step to step symmetry, Journal of Biomechanics 46 (2013) 828–831.

[53] E. Sejdić, C. M. Steele, T. Chau, The effects of head movement on dual-axis cervical accelerometry signals, BMC Reseach Notes 3 (2010) 269.

[54] A. Cohen, J. Kovačević, Wavelets: The mathematical background, Proceedings of the IEEE 84 (1996) 514–522.

Tables

Table 1: Group differences for features in the time domain. Legend - N.S: Not Significant; $\times$: no difference compared to raw data; $\triangle$: HC vs. PN; $\Diamond$: HC vs. PD; $\square$: PD vs. PN; +/-: feature added/removed compared to original data.

	Original	**Corrected**	**Denoised**	**Corrected + denoised**	**Denoised + corrected**
			Standard deviation		
σ_{ML}	N.S.	$\times$	$\times$	$\times$	$\times$
σ_{V}	N.S.	$\times$	$\times$	$\times$	$\times$
σ_{AP}	N.S.	$\times$	$+HC > PD$	$\times$	$\times$
			Skewness		
ξ_{ML}	N.S.	$+PN > HC$	$\times$	$+PN > HC$	$+PN > HC$
ξ_{V}	N.S.	$\times$	$\times$	$\times$	$\times$
ξ_{AP}	N.S.	$\times$	$\times$	$+HC > PD$	$\times$
			Kurtosis		
γ_{ML}	N.S.	$\times$	$\times$	$\times$	$\times$
γ_{V}	N.S.	$\times$	$\times$	$\times$	$\times$
γ_{AP}	N.S.	$\times$	$\times$	$\times$	$\times$
			Cross-correlation		
$\eta_{ML,V}$	$PD > PN$	$-\square$	$\times$	$-\square$	$-\square$
$\eta_{ML,AP}$	N.S.	$\times$	$\times$	$\times$	$\times$
$\eta_{V,AP}$	N.S.	$\times$	$\times$	$\times$	$\times$
			Harmonic ratio		
HR_{ML}	$HC > PD$	$\times$	$-\Diamond$	$-\Diamond$	$-\Diamond$
HR_{V}	$HC > PD$	$+PN > PD$	$\times$	$+PN > PD$	$+PN > PD$
HR_{AP}	$HC > PD$	$+HC > PN$	$\times$	$+HC > PN$	$+HC > PN$

Table 2: Differences between anatomical directions for *statistical features*. For pre-processed data, only the differences with the original data are shown. Legend - N.S: Not Significant; $\times$: no difference compared to raw data; $\triangle$: ML vs. V (ML,V vs. ML,AP for η); $\Diamond$: ML vs. AP (ML,V vs. V,AP for η); $\square$: V vs. AP (ML,AP vs. V,AP for η); +/-: feature added/removed compared to original data

		Original		**Corrected**			**Denoised**			**Corrected + denoised**			**Denoised + corrected**		
	HC	PN	PD	HC	PN	PD	HC	PN	PD	HC	PN	PD	HC	PN	PD
							Standard deviation								
σ		$V > ML$ $AP > ML$ $V > AP$		$\times$ $\times$ $\times$	$\times$ $-\Diamond$ $\times$	$\times$ $-\Diamond$ $\times$		$\times$ $\times$ $\times$		$\times$ $\times$ $\times$	$\times$ $-\Diamond$ $\times$		$\times$ $\times$ $\times$	$\times$ $-\Diamond$ $\times$	
							Skewness								
ξ		$V > ML$ $AP > ML$ $V > AP$		$\times$ $\times$ $\times$	$\times$ $-\Diamond$ $\times$	$\times$ $\times$ $\times$		$\times$ $\times$ $\times$		$\times$ $\times$ $\times$	$\times$ $-\Diamond$ $\times$	$\times$ $\times$ $\times$	$\times$ $\times$ $\times$	$\times$ $-\Diamond$ $\times$	$\times$ $\times$ $\times$
							Kurtosis								
γ	$V > ML$ N.S. N.S.		N.S. N.S. N.S.	$\times$ $\times$ $\times$	$\times$ $\times$ $\times$		$-\triangle$ $\times$ $\times$	$\times$ $+AP > ML$ $\times$	$\times$ $\times$ $\times$	$-\triangle$ $\times$ $\times$	$\times$ $+AP > ML$ $+AP > V$	$\times$ $\times$ $\times$	$-\triangle$ $\times$ $\times$	$\times$ $+AP > ML$ $+AP > V$	$\times$ $\times$ $\times$
							Cross-correlation								
η	N.S. $V,AP > ML,V$ $V,AP > ML,AP$	N.S. $V,AP > ML,V$ $V,AP > ML,AP$	$ML,V > ML,AP$ $V,AP > ML,V$ $V,AP > ML,AP$	$\times$ $\times$ $\times$		$-\triangle$ $\times$ $\times$		$\times$ $\times$ $\times$		$\times$ $\times$ $\times$	$-\triangle$ $\times$ $\times$		$\times$ $\times$ $\times$	$-\triangle$ $\times$ $\times$	
							Harmonic ratio								
HR	$V > ML$ $AP > ML$ N.S.	$V > ML$ $AP > ML$ $V > AP$	$V > ML$ N.S. N.S.	$\times$ $\times$ $+V > AP$	$\times$ -$\Diamond$ $\times$	$\times$ $\times$ $+V > AP$		$\times$ $\times$ $\times$		$\times$ $\times$ $+V > AP$	$\times$ -$\Diamond$ $\times$		$\times$ $\times$ $+V > AP$	$\times$ -$\Diamond$ $\times$	

Table 3: Group differences for frequency features. Legend - N.S: Not Significant; $\times$: no difference compared to raw data; $\triangle$: HC vs. PN; $\Diamond$: HC vs. PD; $\square$: PD vs. PN; +/-: feature added/removed compared to original data

	Original	Corrected	Denoised	Corrected + denoised	Denoised + corrected
			Peak frequency		
f_{pML}	N.S.	$+HC > PD$ $+HC > PN$	$\times$	$\times$	$\times$
f_{pV}	N.S.	$\times$	$\times$	$\times$	$\times$
f_{pAP}	N.S.	$\times$	$\times$	$\times$	$\times$
			Centroid		
f_{cML}	N.S.	$\times$	$\times$	$\times$	$\times$
f_{cV}	N.S.	$\times$	$\times$	$\times$	$\times$
f_{cAP}	$PD > HC$	$+PN > HC$	$-\Diamond$	$+PN > HC$	$+PN > HC$
			Bandwidth		
BW_{ML}	$PD > HC$	$\times$	$\times$	$\times$	$\times$
BW_V	N.S.	$\times$	$\times$	$\times$	$\times$
BW_{AP}	$PD > HC$	$+PN > HC$	$+PN > HC$	$+PN > HC$	$+PN > HC$

Table 4: Differences between anatomical directions for frequency features. For pre-processed data, only the differences with the original data are shown. Legend - N.S: Not Significant; $\times$: no differences compared to the original; $\triangle$: ML vs. V (ML,V vs. ML,AP for η); $\Diamond$: ML vs. AP (ML,V vs. V,AP for η); $\square$: V vs. AP (ML,AP vs. V,AP for η); +/-: feature added/removed compared to original data

		Original			Corrected			Denoised			Corrected + denoised			Denoised + corrected		
		HC	PN	PD	HC	PN	PD	HC	PN	PD	HC	PN	PD	HC	PN	PD
Peak frequency																
f_p		N.S.	$V > ML$			$\times$			$\times$			$\times$		$\times$	$\times$	$\times$
		N.S.	$AP > ML$			$\times$			$\times$			$\times$		$\times$	$\times$	
		N.S.	N.S.			$\times$			$\times$			$\times$		$\times$	$+V > AP$	
Centroid																
f_c		$ML > V$	$ML > V$		$\times$	$\times$	$\times$	$-\triangle$	$-\triangle$	$-\triangle$	$\times$	-$\triangle$	$-\triangle$	$\times$	$-\triangle$	$-\triangle$
		N.S.	N.S		$\times$	$+AP > ML$	$\times$	$\times$	$+AP > ML$	$\times$	$\times$	$+AP > ML$	$\times$	$\times$	$+AP > ML$	$\times$
		N.S.	$AP > V$		$+AP > V$	$\times$	$\times$	$\times$	$\times$	$\times$	$\times$	$\times$	$\times$	$\times$	$\times$	$\times$
Bandwidth																
BW		$ML > V$			$\times$	$\times$		$-\triangle$	$\times$	$\times$	$\times$	$\times$	$\times$	$\times$	$\times$	
		N.S.			$\times$	$+AP > ML$		$\times$	$+AP > ML$	$\times$	$\times$	$+AP > ML$		$\times$	$+AP > ML$	
		$AP > V$			$\times$	$\times$		$\times$	$\times$	$\times$	$\times$	$\times$		$\times$	$\times$	

Figure captions

Figure 1 - Acceleration vectors and their projection in the earth-vertical coordinate system: on the left accelerations in the sagittal plane; on the right accelerations in the coronal plane. $\mathbf{a}_{AP}$, $\mathbf{a}_{ML}$ and $\mathbf{a}_v$ denote the measured accelerations in the AP, ML and V directions respectively.

Figure 2 - Fast wavelet transform algorithm: the signal s goes through a high-pass and a low-pass filter. The resulting signals are downsampled (one sample out of 2 is kept) so as to avoid data redundancy. The approximation signal A_1 and the detail signal D_1 are obtained. The n-level decomposition of the signal is computed by performing the same operation on the approximation signals obtained successively. The decomposition of the signal is given by the sequence $[A_n D_n D_{n-1} \dots D_1]$.

Figure 3 - Comparison of signals before and after tilt correction for a HC control.

Figures

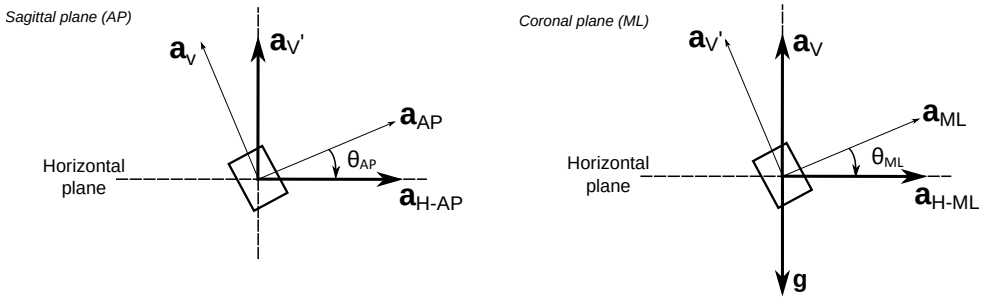

Figure 1: Acceleration vectors and their projection in the earth-vertical coordinate system: on the left accelerations in the sagittal plane; on the right accelerations in the coronal plane. $\mathbf{a}_{AP}$, $\mathbf{a}_{ML}$ and $\mathbf{a}_{v}$ denote the measured accelerations in the AP, ML and V directions respectively.

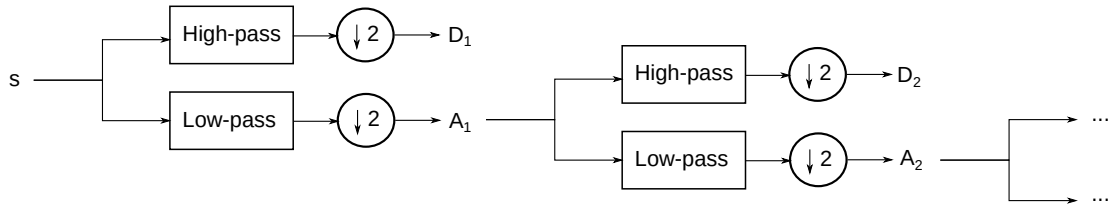

Figure 2: Fast wavelet transform algorithm: the signal s goes through a high-pass and a low-pass filter. The resulting signals are downsampled (one sample out of 2 is kept) so as to avoid data redundancy. The approximation signal A_1 and the detail signal D_1 are obtained. The n-level decomposition of the signal is computed by performing the same operation on the approximation signals obtained successively. The decomposition of the signal is given by the sequence $[A_n D_n D_{n-1} \dots D_1]$.

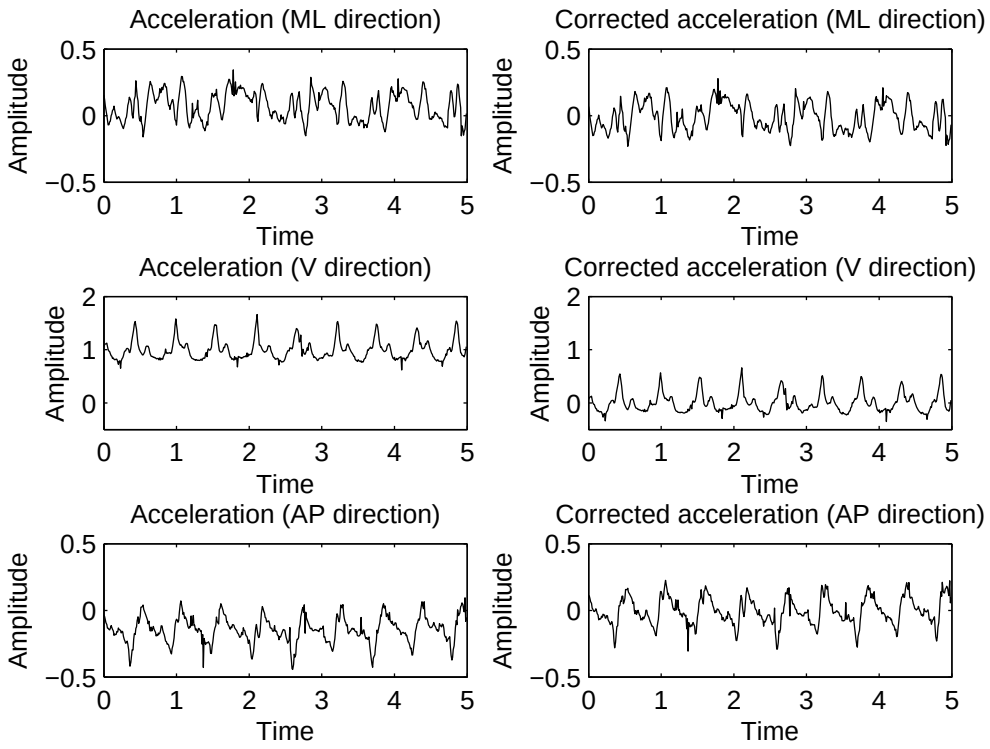

Figure 3: Comparison of signals before and after tilt correction for a HC control